

*Chapter 1***FROM NUCLEI TO NUCLEAR PASTA***C.O. Dorso*<sup>1</sup>, *P.A. Giménez Molinelli*<sup>1</sup> and *J.A. López*<sup>2\*</sup><sup>1</sup>Depto. de Física, FCEN, Universidad de Buenos Aires, Buenos Aires, Argentina<sup>2</sup>University of Texas at El Paso, El Paso, Texas, USA

**PACS** 24.10.Lx, 02.70.Ns **Keywords:** neutron stars, nuclear pasta, nuclear matter, molecular dynamics.

**1. Introduction**

Neutron stars are created as a final product of the death of a massive star. Stars die when the internal thermonuclear fusion can no longer balance the gravitational compression. For such massive stars a supernova shock ejects most of the mass of the star leaving behind a dense core. Since during the collapse a big part of electrons and protons turn into neutrons and escaping neutrinos through electron capture, the residual mass tends to have an excess of neutrons over protons, thus justifying the name of a neutron star.

The mass of a neutron star ranges between 1 and 3 solar masses, its radius is of the order of a  $10^{-5}$  solar radius or about 10 km, which gives it an average density of  $10^{15}$  g/cm<sup>3</sup> or about 20 times that of normal nuclei. Energy considerations indicate [1, 2] that the cores of neutron stars are topped by a crust of about a kilometer thick where the  $\beta$  decayed-produced neutrons form neutron-rich nuclear matter immersed in a sea of electrons.

---

\*E-mail jorgelopez@utep.edu

The density of such crust ranges from normal nuclear density ( $\approx 3 \times 10^{14} \text{ g/cm}^3$ , or  $\approx \rho_0 = 0.15 \text{ nucleons/fm}^3$ ) at a depth of  $\approx 1 \text{ km}$  to the neutron drip density ( $\approx 4 \times 10^{11} \text{ g/cm}^3$ ) at  $\approx 1/2 \text{ km}$ , to, finally, an even lighter mix of neutron-rich nuclei also embedded in a sea of electrons with densities decreasing down to practically zero in the neutron star envelope. The study of the structure of such crust of nuclear matter at subcritical densities, is the purpose of the present work.

It has been shown under different approximations [1, 2, 3, 4, 5, 6, 7, 8, 9] that low-density nuclear matter can exist in the form of non-uniform structures which have been known as “nuclear pastas”. Such effect appears to be due to the interplay between attractive-repulsive nuclear and Coulomb forces. As the density, temperature and proton fraction vary, the stable nuclear shape changes from the uniform phase of the core to configurations with voids filled with a gaseous phase, to “lasagna-like” layers of nuclear matter and gas, to “spaghetti-like” rods of matter embedded in a nuclear gas to “polpetta-like” (meat-ball) clumps to a practically uniformly dissolved gaseous phase [2]. This crust structure is a determining factor in several astronomical processes such as star-quakes, supernova explosions, pulsar frequency and neutrino opacity in supernova matter.

Different models have been used to investigate such low-density phase of nuclear matter [1, 2, 3, 4, 5, 6, 7, 8, 9]. In summary, static models (e.g. liquid-drop model, Thomas-Fermi, Hartree-Fock) find varying structures in nuclear systems using solely energy considerations, i.e. by a balance between the different components of the nuclear and Coulomb energies. Dynamical models, such as quantum molecular dynamics [10, 11], predict the formation of the pasta phases by dynamical means. For complete descriptions of some of these techniques the reader is directed to other chapters of this volume.

Unfortunately, the predictions obtained by these different techniques are somewhat model dependent and a direct comparison between models is not entirely feasible. Such is the case of the effect that the Coulomb interaction between the embedding electron sea and the nuclear charges has on the structure of the nuclear matter. Initially overlooked, such interaction is now known to produce an screening effect that aids the stability of the overall nuclear system while modifying the structure. This interaction, however, can only be included under different approximations [9] depending on the model used.

To provide a practitioner’s introduction to the study of the nuclear pasta, this article presents a brief review of the evolution of the methods used to study nucleon dynamics in Section 2. This is followed with a more complete description of the extension of classical molecular dynamics to infinite systems in Section 2.2. The different techniques used to characterize the nuclear structure, such as cluster recognition algorithms, radial correlation functions and the Minkowski functionals are presented in Section 3. We reach full functionality of the extended *CMD* when the Coulomb interaction is introduced through two common methodologies and its effect on the structure is presented in Section 4. We close the article with some final remarks in Section 5.

## 2. Nucleon dynamics

To study the nuclear structure of stellar crusts is necessary understand the behavior of nucleons, i.e. protons and neutrons, at densities and temperatures as those encountered in the outer layers of stars. This knowledge comes from decades of study of nucleon dynamics

through the use of computational models that have evolved from simple to complex. In this section we review this evolution presenting a synopsis of existing models and culminating with the model used in this work, namely classical molecular dynamics (*CMD*).

## 2.1. Evolution of models

Several approaches have been used to simulate the behavior of nuclear matter, especially in reactions. The initial statistical studies of the 1980's, which lacked fragment-fragment interactions and after-breakup fragment dynamics [12], were followed in the early 1990s by more robust studies that incorporated these effects. All these approaches, however, were based on idealized geometries and missed important shape fluctuation and reaction-kinematic effects. On the transport-theory side, models were developed in the late 1990s based on classical, semiclassical and quantum-models; because of their use in the study of stellar nuclear systems nowadays, a side-by-side comparison of these transport models is in order.

Starting with the semiclassical, a class of models known generically as *BUU* is based on the Vlasov-Nordheim equation [13] also known as the Boltzmann-Uehling-Uhlenbeck [14]. These models numerically track the time evolution of the Wigner function,  $f(\vec{r}, \vec{p})$ , under a mean potential  $U(\vec{r})$  to obtain a description of the probability of finding a particle at a point in phase space. The semiclassical interpretation constitutes *BUU*'s main advantage; the disadvantages come from the limitation of using only a mean field which does not lead to cluster formation. To produce fragments, fluctuations must be added by hand, and more add-ons are necessary for secondary decays and other more realistic features.

On the quantum side, the molecular dynamics models, known as *QMD*, generically speaking, solve the equations of motion of nucleon wavepackets moving within mean fields (derived from Skyrme potential energy density functional). The method allows the imposition of a Pauli-like blocking mechanism, use of isospin-dependent nucleon-nucleon cross sections, momentum dependence interactions and other variations to satisfy the operator's tastes. The main advantage is that *QMD* is capable of producing fragments, but at the cost of a poor description of cluster properties and the need of sequential decay codes external to *BUU* to "cut" the fragments and de-excite them [15]; normally clusters are constructed by a coalescence model based on distances and relative momenta of pairs of nucleons. Variations of these models applied to stellar crusts can be found elsewhere in this volume.

Of particular importance to this article is the classical molecular dynamics (*CMD*) model, brainchild of the Urbana group [16] and designed to reproduce the predictions of the Vlasov-Nordheim equation while providing a more complete description of heavy ion reactions. As it will be described in more detail in the next section, the model is based on the Pandharipande potential which provides the "nuclear" interaction through a combination of Yukawa potentials selected to correspond to infinite nuclear matter with proper equilibrium density, energy per particle and compressibility.

Problems common to both *BUU* and *QMD* are the failure to produce appropriate number of clusters, and the use of hidden adjustable parameters, such as the width of wavepackets, number of test particles, modifications of mean fields, effective masses and cross sections. These problems are not present in the classical molecular dynamics model which,

without any adjustable parameters, hidden or not, is able to describe the dynamics of the reaction in space from beginning to end and with proper energy, space and time units. It intrinsically includes all particle correlations at all levels, i.e. 2-body, 3-body, etc. and can describe nuclear systems ranging from highly correlated cold nuclei (such as two approaching heavy ions), to hot and dense nuclear matter (nuclei fused into an excited blob), to phase transitions (fragment and light particle production), to hydrodynamics flow (after-breakup expansion) and secondary decays (nucleon and light particle emission).

The only apparent disadvantage of the *CMD* is the lack of quantum effects, such as the Pauli blocking, which at medium excitation energies stops the method from describing nuclear structure correctly. Fortunately, in collisions, the large energy deposition opens widely the phase space available for nucleons and renders Pauli blocking practically obsolete [17], while in stellar environments, at extremely low energies and with frozen-like structures, momentum-transferring collisions cease to be an important factor in deciding the stable configuration of the nuclear matter. Independent of that, the role of quantum effects in two body collisions is guaranteed to be included by the effectiveness of the potential in reproducing the proper cross sections, furthermore, an alternate fix is the use of momentum dependent potentials (as introduced by Dorso and Randrup [18]) when needed.

Although no theories can yet claim to be a perfect description of nuclear matter, all approaches have their advantages and drawbacks and, if anything can be said about them, is that they appear to be complementary to each other.

## 2.2. Classical Molecular Dynamics

Out of the techniques used to describe nuclear matter, only classical molecular dynamics can describe all limiting behavior such as non-equilibrium dynamics, hydrodynamic flow, as well as changes of phase. The method was introduced decades ago to study restrictive aspects of nuclear reactions [19, 20], but was refined for realistic heavy-ion collisions and infinite-matter properties by Pandharipande and coworkers [21].

In a nutshell, the classical molecular dynamics method considers the participating nucleons as classical particles interacting through a two-body potential. By solving the coupled equations of motion of the many-body system numerically, the *CMD* technique can approximate the time evolution of hundreds or thousands of interacting nucleons to study either reactions or the structure of infinite nuclear matter from a microscopic point of view.

A key ingredient of the *CMD* technique is the interaction potential. In the past, initial studies were based on argon-like 6-12 potentials [22], followed by skyrme-type potentials [23], until more phenomenologically correct interactions were developed by Pandharipande [21]. The resulting two-body potentials were crafted as to reproduce the empirical energy and density of nuclear matter, as well as realistic effective scattering cross sections.

In general terms, the *MD* investigations of confined nuclear matter consist of placing “nucleons” in a container at a desired density and endowed with a distribution of velocities as to mimic a maxwellian distribution of energy. After following the trajectories of motion until thermal equilibrium is achieved, the system is force-heated or cooled to reach a desired temperature. Recording the position and velocities of each nucleon allows then to use fragment-recognition algorithms to identify clusters. The same procedure can be implemented to study reaction between two colliding “nuclei”, as well as for expanding

systems.

For the case of interest, i.e. for infinite systems composed of a given ratio of protons to neutrons, a similar procedure can be implemented using molecular dynamics in containers under periodic boundary conditions to simulate infinite systems.

### 2.2.1. The potential

The molecular dynamics model used in the present study was first introduced in 1999 [24], and ever since has been very fruitful in nuclear studies of, among other phenomena, neck fragmentation [25], phase transitions [26, 27], and isoscaling [28, 29, 30, 31, 32, 33, 34]; all without any adjustable parameters. Readers are directed to these references for further details on the model; here only a brief synopsis will be presented.

The nuclear interaction potentials [16] guarantee that the system will have nuclear-like properties such as proper binding energy, radii and nucleon-nucleon cross sections. The explicit expressions of the potential is:

$$\begin{aligned} V_{np}(r) &= V_r [exp(-\mu_r r)/r - exp(-\mu_r r_c)/r_c] \\ &\quad - V_a [exp(-\mu_a r)/r - exp(-\mu_a r_a)/r_a] \\ V_{NN}(r) &= V_0 [exp(-\mu_0 r)/r - exp(-\mu_0 r_c)/r_c] . \end{aligned}$$

The Pandharipande potentials differentiate between different types of nucleons:  $V_{np}$  is the potential between a neutron and a proton and it is attractive at large distances and repulsive at small ones, and  $V_{NN}$  is the interaction between identical nucleons and it is purely repulsive; notice that no bound state of identical nucleons can exist.

In terms of parameters, the cutoff radius used is  $r_c = 5.4 \text{ fm}$  after which the potentials are set to zero, i.e.  $V_{NN}(r > r_c) = V_{np}(r > r_c) = 0$ . Two different sets of parameters for the Yukawa potentials  $\mu_r$ ,  $\mu_a$  and  $\mu_0$ , were developed [16] and correspond to infinite-nuclear matter systems with an equilibrium density of  $\rho_0 = 0.016 \text{ fm}^{-3}$ , a binding energy  $E(\rho_0) = 16 \text{ MeV/nucleon}$  and compressibility of about  $250 \text{ MeV}$  ("Medium") or  $535 \text{ MeV}$  ("Stiff"). It should be remarked that, at a difference from potentials used by other models [10], the potential used here has a hard core not present in other approximations.

### 2.2.2. Ground state nuclei

Although the  $T = 0$  state of this classical nuclear matter is a simple cubic solid, nuclear systems can be mimicked by adding enough kinetic energy to the nucleons. To study nuclei, for instance, liquid-like spherical drops with the right number of protons and neutrons are constructed confined in a steep spherical potential and then brought to the "ground" state by cooling them slowly from a rather high temperature until they reach a self-contained state. Removing then the confining potential the system is further cooled down until a reasonable binding energy is attained, the remaining kinetic energy of the nucleons helps to resemble the Fermi motion. Figure 1 shows the binding energies of "ground-state nuclei" obtained with the mass formula and with *CMD*; see [34] for details.

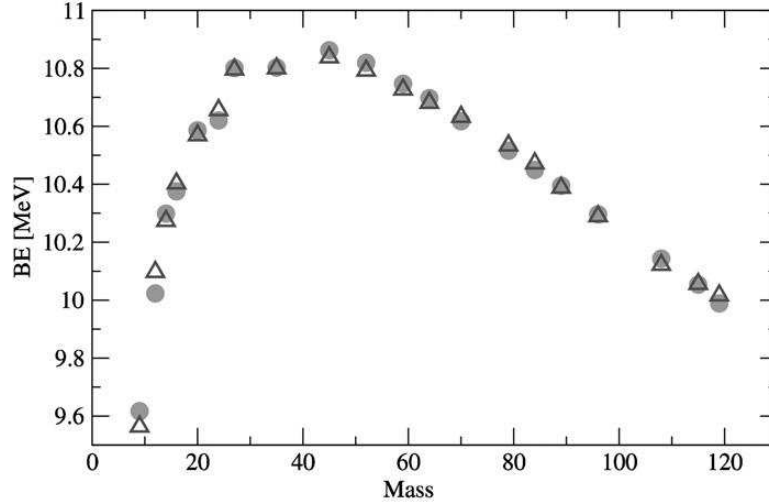


Figure 1. Binding energies of ground-state nuclei obtained with mass formula fit (triangles) for the Stiff model with the corresponding ground states calculated using *CMD* (circles).

### 2.2.3. Collisions

With respect to collisions, these potentials are known to reproduce nucleon-nucleon cross sections from low to intermediate energies [16] and it has been used extensively in studying heavy ion collisions (see e.g. [25, 27]). For such reactions, two “nuclei” are boosted against each other at a desired energy. From collision to collision, the projectile and target are rotated with respect to each other at random values of the Euler angles. The evolution of the system is followed using a velocity-Verlet algorithm with energy conservation better than 0.01%. At any point in time, the nucleon information, position and momenta, can be turned into fragment information by identifying the clusters and free particles; several such cluster recognition algorithms have been developed by our collaborator, C.O. Dorso, and they are well described in the literature [35, 36].

The method yields mass multiplicities, momenta, excitation energies, secondary decay yields, etc. comparable to experimental data [37, 25]. Figure 2, for instance, shows experimental and simulated parallel velocity distributions for particles obtained from mid-peripheral and peripheral  $^{58}\text{Ni} + C$  collisions performed at the Coupled Tandem and Super-Conducting Cyclotron accelerators of AECL at Chalk River [25].

### 2.2.4. Thermostatic properties of nuclear matter

To study thermal properties of static nuclear matter, be these drops or infinite systems, nucleons are positioned at random, but with a selected density, in a container and “heated”. After equilibration, the system can then be used to extract macroscopic variables. Repeating these simulations for a wide range of density and temperature values, information about the energy per nucleon,  $\epsilon(\rho, T)$ , can be obtained and used to construct analytical fits in the spirit of those pioneered by Bertsch, Siemens and Kapusta [38, 39, 40, 17]; these fits in turn can

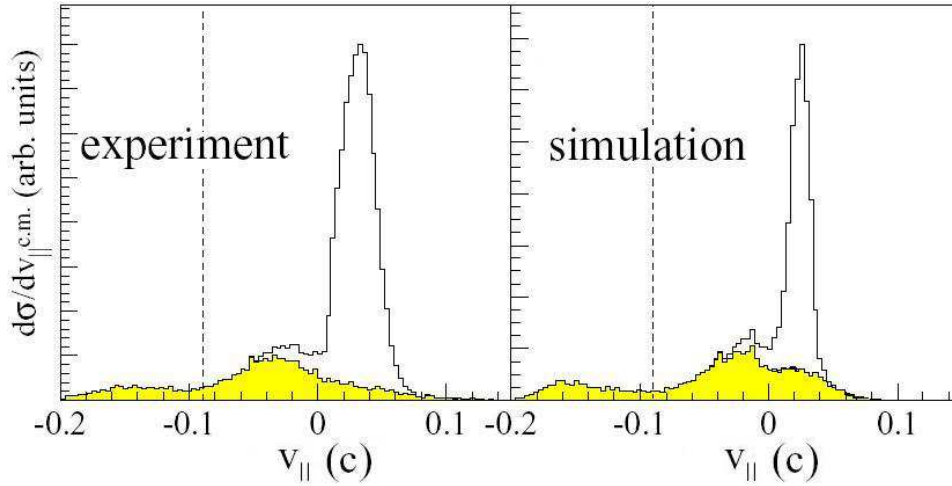


Figure 2. Experimental and simulated parallel velocity distributions for  $^{58}\text{Ni}+C$  collisions.

be used to derive other thermodynamical variables such as pressure, etc.

The left panel of Figure 3 shows the results of the method as applied by Pandharipande and coworkers [16] for stiff cold infinite nuclear matter with the squares representing *CMD* calculations ( $E$ ) and the line a polynomial fit ( $E_p$ ). For finite systems, the right panel of the same figure demonstrates the feasibility of using *CMD* to study thermal properties such as the caloric curve (i.e. the temperature - excitation energy relationship) for a system of 80 nucleons equilibrated at four different densities; see [34] for complete details.

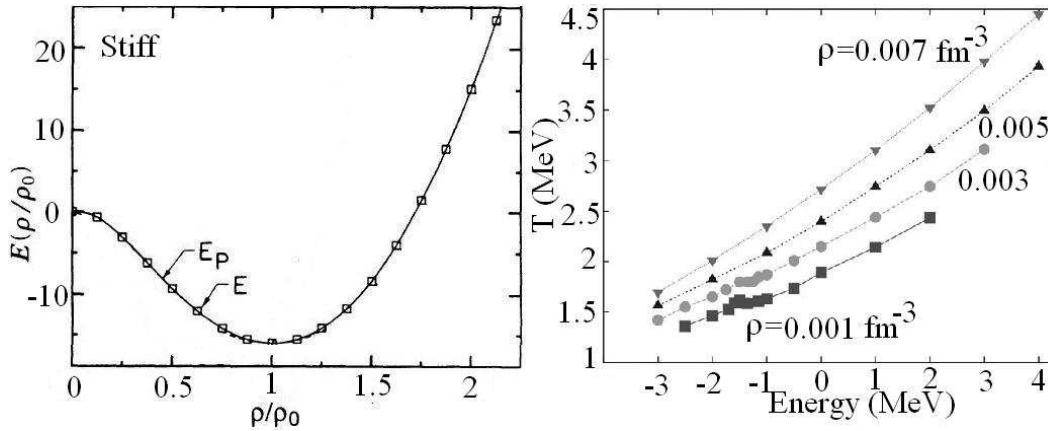


Figure 3. Left panel: Energy per particle of stiff cold matter calculated with *CMD* and a polynomial fit. Right panel: Caloric curve of a system equilibrated at four different densities as calculated by *CMD*.

After having reviewed the different characteristics of *CMD* as well as several of its applications, we now turn to its use in the study of nuclear structures in infinite media.

### 3. Structure of stellar crusts

To study infinite systems, such as stellar crusts, *CMD* is applied to systems confined in a cell surrounded with replicas to avoid finite-size effects. The systems studied were endowed with a fixed proton-to-neutron ratios of either  $x = Z/A = 0.3$  or  $0.5$  and, to always maintain a sizable proton number, this was kept at a constant 1000 while increasing the total number of nucleons to  $A = 2000$  and  $3333$  in the two different values of  $x$ , respectively. As a consequence of the variation of the total nucleon number, the size of the box was adjusted as to achieve the desired densities; these varied between  $\rho = 0.01 \text{ fm}^{-3}$  (or  $\approx \rho_0/15$ ) all the way to almost  $\rho_0$ .

The systems constructed are confined systems placed in a closed cubical container at a fixed density and proton ratio  $x$  and allowed to equilibrate at a low temperature. The excitation energy is added to such system by scaling the momenta of the particles. The trajectories of individual nucleons are then obtained using an standard Verlet algorithm with an energy conservation of  $\mathcal{O}(0.01\%)$ .

The final configurations of the system were obtained at low temperature of  $T = 0.1 \text{ MeV}$  by means of the isothermal molecular dynamics prescribed by the Andersen thermostat procedure [41]. Our technique gradually cools the system in small temperature steps (say  $0.02 \text{ MeV}$ ) while reaching thermal equilibrium at every step; although a temperature of  $0.1 \text{ MeV}$  is rather large for stellar crusts, in terms of the dynamics of nucleons, it practically corresponds to a frozen state.

#### 3.1. Temperature and nuclear matter structure

To illustrate both the effect temperature has on the nucleon dynamics as well as the manner in which *CMD* operates, it is pedagogically useful to present the structure of nuclear systems at varying temperatures. Figure 4 shows the formation of a final structure with  $x = 0.5$  and  $\rho = 0.55 \text{ fm}^{-3}$  using the screened Coulomb potential (to be presented in the next section) as the system cools down from  $T = 1.0 \text{ MeV}$  to  $T = 0.1 \text{ MeV}$ .

#### 3.2. Characterizing the structure of nuclear matter

Once a configuration is achieved, the nucleon information is recorded to provide the position and momentum of the nucleons during the evolution. Such microscopic information can be used to identify clusters as well as to characterize the structure of nuclear matter by means of the liquid structure function and the Minkowski functionals.

##### 3.2.1. Cluster recognition

The nucleon positions and momenta are used to identify the fragment structure of the system by means of the "Minimum Spanning Tree" (*MST*) cluster-detection algorithm of [42] and refined by [36]. In summary, *MST* looks for correlations in configuration space: a particle  $i$  belongs to a cluster  $C$  if there is another particle  $j$  that belongs to  $C$  and  $|r_i - r_j| \leq r_{cl}$ , where  $r_{cl}$  is a clusterization radius which, for the present study, was set to  $r_{cl} = 3.0 \text{ fm}$ .

The main drawback of *MST* is that, since only correlations in  $r$ -space are used, it neglects completely the effect of momentum giving incorrect information for dense sys-

tems and for highly dynamical systems such as those formed in colliding nuclei. Although more robust algorithms which look at relative momenta between nucleons or pair-binding energies have been devised for such systems (e.g. as the "Early Cluster Recognition Algorithm", *ECRA* [18]), in the case of relatively cold systems, such as nuclear crusts, the *MST* is sufficient. In our case of periodic boundary conditions, the *MST* detection of fragments has been modified to take into account the image cells and recognize fragments that extend into adjacent cells.

The Figure 5 shows an example of the size distribution of the clusters obtained for a case with 3,333 nucleons,  $x = 0.3$ , and at  $T = 0.3 \text{ MeV}$  and  $\rho = 0.009 \text{ fm}^{-3}$ . The inset shows a projection of the position of the nucleons within the cell. The shown structure was obtained with the "screened Coulomb" treatment that will be described in the next section.

### 3.2.2. Pair correlation function

A further characterization of the structure of nuclear matter is based on the liquid structure function,  $S(k)$ , which quantifies the density fluctuations.  $S(k)$  is obtained from the pair correlation function,  $g(r)$ , which is the ratio of the average local density to the global density,  $g(r) = \rho(r)/\rho_0$ .

The structure function is related to the Fourier spectrum of the density fluctuations

$$S(k) = (V/\rho_0) \langle \rho_k \rho_{-k} \rangle,$$

where  $\rho_k$  denotes the Fourier transform of  $\delta\rho(r)$ . This function can be obtained from the pair correlation function  $g(r)$  through

$$S(k) = 1 + \rho \int d^3r \exp(i\mathbf{k} \cdot \mathbf{r}) [g(r) - 1].$$

For computing purposes, the pair correlation function  $g(r)$  is taken as the conditional probability density of finding a particle at  $\mathbf{r}_i + \mathbf{r}$  given that there is one particle at  $\mathbf{r}_i$ . It gives information about the spatial ordering, or structure, of a system of particles. Formally,

$$g(r) = \frac{V}{4\pi r^2 N^2} \left\langle \sum_{i \neq j} \delta(r - r_{ij}) \right\rangle,$$

where  $r_{ij}$  is  $|r_i - r_j|$ . For our case, this was calculated by constructing histograms of the distances between particles for several configurations and then averaging them. To keep calculation times reasonable, but still attain accuracy at ranges adequate to the study of the nuclear matter structure, we considered particles (and their images) satisfying  $r_{ij} \leq 1.5L$  with  $L$  the simulation box size.

The Figure 6 shows an example of the radial correlation function obtained for a case with 2,000 nucleons,  $x = 0.5$ , and at  $T = 0.1 \text{ MeV}$  and  $\rho \approx 0.043\rho_0$ . The inset shows three dimensional depiction of the position of the nucleons in the  $L = 28.77 \text{ fm}$  cell; again, this structure was obtained with the "screened Coulomb" treatment.

### 3.2.3. Minkowski functionals

Yet another method to characterize the morphology of three-dimensional patterns in terms of geometrical and topological descriptors are the Minkowski functionals. Here a brief practitioner's guide will be presented; for a full description of the method, the reader is directed to [43].

The basic goal of the Minkowski functionals is to characterize the topology of a distribution of points by means of quantifying connected points as well as empty spaces; for this the patterns are embedded in a uniform grid. For our case of a large number of particles, the technique is applied by placing a grid inside the *CMD* cell and take the occupied grid cells as filled and those not occupied as empty. Once this grid has been created the Euler characteristic  $\chi$  can be obtained as follows.

In general,  $\chi$  equals the number of regions of connected grid cells minus the number of completely enclosed regions of empty grid cells. Two grid cells are connected if they are immediate neighbors, next-nearest neighbors, or are connected by a chain of occupied grid cells. Characterizing the connected structure by its number of occupied cubes,  $n_c$ , faces,  $n_f$ , and vertices,  $n_v$ , including possible contributions from the interior of the structure, the Minkowski functionals can be calculated through

$$V = n_c, S = -6n_c + 2n_f, 2B = 3n_c - 2n_f + n_c, \chi = -n_c + n_f - n_c + n_v$$

Figure 7 shows an example of a nuclear structure, the cubic grid enclosing it, and the values of the Minkowski functionals. For the computational aspects, the reader is directed to [43].

## 4. The Coulomb problem

A major difference between the study of nucleon dynamics in reactions and in stellar crusts is the presence of an embedding electron sea. The nuclear system created in the outer part of a neutron star is expected to be embedded in a relativistic degenerate gas of electrons resulting from the large number of weak decay processes that took place during the collapse-driven supernova explosion. The electron gas effectively renders the system neutral and  $\beta$ -equilibrated.

The balance between nuclear and Coulomb interactions which stabilize spherical nuclei is modified in the presence of the electron gas. The nuclear matter, be this in any type of shape or form, now feels the additional Coulomb interactions of the electron gas, which provides an effective screening and an overall reduction of the Coulomb energy of felt by the protons. The main effect of these energy shifts is to modify the preferred nuclear matter structure for a given density-temperature region; given the infinite range of the Coulomb interaction some approximation is needed when taking this effect into account in either static or dynamical models; the effect has been studied, for instance, using a  $T = 0$  liquid-drop model [44], or with *QMD* using a screened Coulomb potential [7] or an Ewald summation procedure [45].

The fact that the results of these Coulomb calculations appear to be model dependent [45] motivated us to present in this review the two most common approaches, screened potential and Ewald summation, using the same dynamical model, *CMD*. Concisely, the *CMD* model of protons and neutrons will now be assumed to be immersed in a uniform

gas of non-interacting electrons with the exact electron density needed to guarantee charge neutrality. The only effect of this sea of electrons is to add an overall Coulomb interaction to the nuclear potential, and take into account its effect in the equations of motion; for this we use two strategies, Thomas-Fermi Screening and Ewald Summations, which are now described in turn.

#### 4.1. Thomas-Fermi Screening

The Thomas-Fermi Screening model of the Coulomb interaction takes the electron gas as an ideal Fermi gas at the same number density as the protons. This electron gas, being uniform, does not exert any force on protons but becomes polarized in their presence effectively “screening” the proton charge.

In this framework, the Coulomb interaction can be included in the equations of motion for nucleons by means of the screened Coulomb potential obtained from solving the Poisson equation. This procedure yields a potential of the form:

$$V_C^{(Scr)}(r) = \frac{e^2}{r} \exp(-r/\lambda)$$

where  $\lambda$  is a screening length which effectively turns the Coulomb potential into a finite-range potential suitable for our *MD* calculations. The relativistic Thomas-Fermi screening length is given by

$$\lambda = \frac{\pi^2}{2e} \left( k_F \sqrt{k_F^2 + m_e^2} \right)^{-\frac{1}{2}}$$

where  $m_e$  is the electron mass, the electron Fermi momentum is given by  $k_F = (3\pi^2\rho_e)^{1/3}$ , and  $\rho_e$  is the electron gas number density (taken equal to that of the protons). To avoid finite size effects,  $\lambda$  should be significantly smaller than the size of the simulation cell,  $L = (A/\rho)^{1/3}$ , but since  $\lambda$  depends on the density of the system, it is always possible to satisfy this condition by increasing the simulation box size along with the number of particles. However, since this can lead to prohibitively large systems for our current computation capabilities, we follow the prescription given in [10] and set  $\lambda = 10 fm$ .

To compare to the results obtained with the Ewald summation to be presented in the following section, figures 8 and 9 present on the left column representative structures obtained with symmetric nuclear matter ( $x = 0.5$ ) using the screened Coulomb method. For clarity, the figures exclude free particles and show only the connected structures with four nucleons or more.

#### 4.2. Ewald Summation

The Ewald summation technique is widely used to compute long range interactions; in this case, the background electron gas plays a more subtle but equally essential role. In this approach, each proton is surrounded by a Gaussian charge distribution of equal magnitude and opposite sign that screens the original. Each of these Gaussians is likewise cancelled by opposing distributions. This allows for the problem to be split in two: a short-ranged interaction between screened charges, and an infinite periodic system of Gaussian charges

that can be solved in reciprocal space using Fourier transforms. We refer the reader to [46, 47] for details on the derivation.

The screening Gaussian distributions exactly compensate the proton charge and have a width set by a parameter  $\alpha$ :

$$\rho_{Gauss}(r) = -e \left( \frac{\alpha}{\pi} \right)^{\frac{3}{2}} \exp(-\alpha r^2)$$

where  $e$  is the charge of a single proton. The real space part of the contribution to the Coulomb potential energy takes the form

$$U_{Ewald}^{Real} = \frac{e^2}{2} \sum_{i \neq j}^Z \frac{\text{erfc}(\sqrt{\alpha} r_{ij})}{r_{ij}} - \left( \frac{\alpha}{\pi} \right)^{\frac{1}{2}} \sum_{i=1}^Z e^2$$

where  $Z$  is the number of protons and  $\text{erfc}(x)$  the complementary error function. The last (constant) term is a correction for a “self interaction” between each proton and its Gaussian partner. The parameter  $\alpha$  controls the range of the short range effective potential of the screened proton.

The contribution to the energy of the remaining charge distributions is given by

$$U_{Ewald}^{Fourier} = \frac{1}{2V} \sum_{\mathbf{k} \neq 0}^{k_{co}} \frac{4\pi}{k^2} |\rho(\mathbf{k})|^2 \exp\left(-\frac{k^2}{4\alpha}\right) \quad (1)$$

where

$$\rho(\mathbf{k}) = \sum_{j=1}^Z \exp(i\mathbf{k} \cdot \mathbf{r}_j)$$

is the structure factor.

The summation in Eq. (1) runs over all reciprocal space vectors ( $\mathbf{k} = \frac{2\pi}{L}(n_x, n_y, n_z)$  with  $n_i$  integers) inside a sphere defined by the cutoff  $k_{co}$ . The problematic term with  $k = 0$  corresponds to a polarization energy that banishes because of infinite polarizability of the background electron gas.

The Fourier space part is by far the most time consuming part of the simulation. The choice of  $\alpha$  and  $k_{co}$  is crucial to balance the length and the accuracy of a simulation. We chose  $\alpha$  so that the range of the real space Ewald sum matches that of the nuclear part and  $k_{co} = \frac{2\pi}{L} n_c$  with  $n_c = 8$ . This guarantees a relative error in the energy of  $\mathcal{O}(10^{-6})$ .

Figures 8 and 9 show representative structures obtained with symmetric nuclear matter ( $x = 0.5$ ) using the Ewald summation method with systems at densities varying between  $0.09\rho_0 < \rho < 0.5\rho_0$ . As in the previous figures, free particles are not included and only connected structures with four nucleons or more are shown.

### 4.3. Discussion

The differences of the structures obtained with the screened Coulomb method and the Ewald summation technique are readily noticeable. The screened potential allowed the formation of the whole menu of pasta types, from polpetta at low densities, to spaghetti, to lasagna, gnocci and to sciaciatia (Italian meat pie, i.e. a uniform state with holes) at higher densities.

Comparing to previous results (at lower values of  $x$ ) we observe a similar evolution of the structures but at different values of the density. Ref. [2], for instance, produces uniform states with holes (scaciatta) at  $0.6\rho_0 - 0.7\rho_0$  while here such structure is observed at  $0.4\rho_0 - 0.5\rho_0$ , we find the lasagna-type layers between  $0.2\rho_0 - 0.3\rho_0$  while studies using Wigner-Seitz [2] cells place such a structure at  $0.4\rho_0 - 0.5\rho_0$  and even at  $0.105\rho_0$  [45], likewise we observe the spaghetti and meatballs phases at  $0.05\rho_0 - 0.15\rho_0$  while other studies [45] obtain such structures at  $0.06\rho_0 - 0.09\rho_0$ .

The structures obtained with the Ewald summation presented a much reduced menu. Spaghetti rods appeared briefly at very low densities ( $0.03\rho_0 - 0.1\rho_0$ ), spätzle-like or gnocci-like structure at intermediate densities ( $0.15\rho_0 - 0.2\rho_0$ ), and scaciatta at all other higher densities ( $> 0.3\rho_0$ ).

The differences between the results obtained with different Coulomb approximations evidence the need to use a proper method to evaluate the Coulomb interaction of the electron gas. The extension of this study to other proton ratios and other temperatures is in progress; preliminary results indicate that neutron-rich matter (with  $x = 0.3$ ) has a reduced range of possibilities, mostly limited to lasagna-like and gnocci-like structures. These and other results of the present study (pair correlation function, fragment distribution, free neutrons, Minkowski functionals, etc.) will be published elsewhere in the near future.

## 5. Final remarks

Neutron stars have a crust composed of neutron-rich nuclear matter immersed in a sea of electrons. At subnormal densities, the structure of such crust is determined by a fine balance of nuclear and electric forces, and it goes from a uniform consistency at normal densities, to a “clumpy” texture, to rod-like, and to layer-like as the density decreases. Such structures have been studied with static and dynamic models, and in this article the classical molecular dynamics model is used to illustrate several features of this “nuclear pasta”.

The *CMD* has been extremely successful to reproduce many features of cold nuclei, nucleon scattering, as well as heavy ion collisions; its extension to infinite systems allows its application to stellar crusts. The study of the pasta phases requires the use of cluster recognition algorithms, radial correlation functions and other topological instruments, such as the Minkowski functionals. Other required techniques are tools to introduce the effect of the electron sea into the *CMD* equations of motion, we reviewed two such methods: the screened Coulomb potential and the Ewald summation and found substantial differences in the structures formed under the two methods: those formed with the screened potential ARE much richer in variety than those obtained with the Ewald summation.

An implicit result is the fact that the *CMD* is a computationally efficient method to study the nuclear pasta.

## Acknowledgments

C.O.D. is a member of the “Carrera del Investigador” CONICET supported by the Universidad de Buenos Aires, CONICET through grant PIP5969. J.A.L Acknowledges support

from grant NSF-PHY 1066031. J.A.L. thanks Dr. Jorge Piekarewicz for suggesting the use of *CMD* to study the nuclear pasta.

## References

- [1] D. G. Ravenhall, C. J. Pethick and J. R. Wilson, Phys. Rev. Lett. **27**, 2066 (1983).
- [2] K. Oyamatsu, Nucl. Phys. **A561**, 431 (1993).
- [3] M. Hashimoto, H. Seki and M. Yamada, Prog. Theor. Phys. **71**, 320 (1984).
- [4] R. D. Williams and S. E. Koonin, Nucl. Phys. **A435**, 844 (1985).
- [5] C. P. Lorentz, D. G. Ravenhall and C. J. Pethick, Phys. Rev. Lett. **25**, 379 (1993).
- [6] K. S. Cheng, C. C. Yao and Z. G. Dai, Phys. Rev. **C55**, 2092 (1997).
- [7] T. Maruyama, K. Niita, K. Oyamatsu, T. Maruyama, S. Chiba and A. Iwamoto, Phys. Rev. **C57**, 655 (1998).
- [8] T. Kido, T. Maruyama, K. Niita and S. Chiba, Nucl. Phys. **A663-664**, 877 (2000).
- [9] G. Watanabe, K. Iida and K. Sato, Nucl. Phys. **A676**, 445 (2000).
- [10] C. J. Horowitz, M. A. Perez-Garcia, and J. Piekarewicz, Phys. Rev. **C69**, 045804 (2004)
- [11] G. Watanabe, K. Sato, K. Yasuoka and T. Ebisuzaki, Phys. Rev. **C66**, 012801 (2002)
- [12] H.W. Barz, J.P. Bondorf, D. Idier, and I.N. Mishustin, Phys. Lett. **B382**, 343 (1996).
- [13] L.W. Nordheim, Proc. R. Soc. London, **A119**, 689 (1928).
- [14] E.A. Uehling and G.E. Uhlenbeck, Phys. Rev. **43**, 552 (1933).
- [15] A. Polanski et al., Radiat. Prot. Dosimetry, **115**, (2005).
- [16] R. J. Lenk, T. J. Schlagel and V. R. Pandharipande, Phys. Rev. **C42**, 372 (1990).
- [17] J.A. López and C.O. Dorso, Lecture Notes on Phase Transformations in Nuclear Matter, World Scientific, Hackensack, NJ, USA, ISBN 978-981-02-4007-3 (2000).
- [18] C. O. Dorso and J. Randrup, Phys. Lett. **B301**, 328 (1993).
- [19] L. Wilets, E.M. Henley, M. Kraft and A.D. Mackellar, Nuc. Phys. **A282**, 341 (1977).
- [20] A.R. Bodmer and C.N. Panos, Phys. Rev. **C15**, 1342 (1977).
- [21] R. J. Lenk and V. R. Pandharipande, Phys. Rev. **C34**, 177 (1986); A. Vicentini, G. Jacucci and V. R. Pandharipande, Phys. Rev. **C31**, 1783 (1985).
- [22] B. Friedman and V. R. Pandharipande, Nuc. Phys. **A361**, 502 (1981).

- 
- [23] J.A. López and G. Lübeck, Phys. Lett. **B219**, 215 (1989).
- [24] A. Barrañón, C. O. Dorso, J. A. López and J. Morales, Rev. Mex. Fís. **45**, 110 (1999).
- [25] A. Chernomoretz, L. Gingras, Y. Larochelle, L. Beaulieu, R. Roy, C. St-Pierre and C. O. Dorso, Phys. Rev. **C65**, 054613 (2002).
- [26] A. Barrañón, C. O. Dorso and J. A. López, Rev. Mex. Fís. **47-Sup. 2**, 93 (2001).
- [27] A. Barrañón, C. O. Dorso, and J. A. López, Nuclear Phys. **A791**, 222 (2007).
- [28] C. O. Dorso, C. R. Escudero, M. Ison and J. A. López, Phys. Rev. **C73**, 044601 (2006).
- [29] A. Dávila, C. Escudero, J. A. López and C. O. Dorso, Physica **A 374**, 663 (2007).
- [30] C. O. Dorso, Phys. Rev. **C73**, 034605 (2006).
- [31] L. Moretto, C. O. Dorso, L. Phair and J.B.Elliott, Phys. Rev. **C77**, 037603 (2008).
- [32] C. O. Dorso, C. M. Hernández, J. A. López and J. A. Muñoz, Phys. Rev. **C78**, 034613 (2008).
- [33] J. A. López, J. A. Muñoz and C. O. Dorso, Rev. Mex. Fís. **S 56 (1)**, 85-88 (2010).
- [34] C.O. Dorso, P. Giménez-Molinelli and J.A. López, J. Phys. G: Nucl. Part. Phys. **38** 115101 (2011); C.O. Dorso, P.A. Giménez Molinelli and J.A. López, Rev. Mex. Phys., **S 57 (1)**, 14 (2011).
- [35] C. O. Dorso and J. Aichelín, Phys. Lett. **B345**, 197 (1995).
- [36] A. Strachan and C.O. Dorso, "Time scales in fragmentation", Phys. Rev. **C55**, 775 (1997); *ibid*, "Fragment recognition in molecular dynamics", Phys. Rev. **C56**, 995 (1997).
- [37] M. Belkacem et al., "Searching for the nuclear liquid-gas phase transition in Au+Au collisions at 35 MeV/nucleon", Phys. Rev. **C54**, 2435 (1996).
- [38] G. F. Bertsch and P. Siemens, Nuc. Phys. **A314**, 465 (1984).
- [39] J. Kapusta, Phys. Rev. **C29**, 1735 (1984).
- [40] J. López and P. Siemens, "Nuclear Fragmentation", Nuc. Phys. **A431**, 728 (1984).
- [41] H.C. Andersen, J. Chem. Phys. **72** 2384 (1980).
- [42] T.L. Hill, J. Chem. Phys. **23**, 617 (1955).
- [43] K. Michielsen and H. De Raedt, Phys. Reports **347**, 461 (2001).
- [44] G. Watanabe and K. Iida, Phys. Rev. **C68**, 045801 (2003).
- [45] G. Watanabe, K. Sato, K. Yasuoka and T. Ebisuzaki, Phys. Rev. **C68**, 035806 (2003).

- [46] D. Frenkel and B. Smit, "Understanding Molecular Simulations", 2nd Ed., Academic Press (2002).
- [47] T. M. Nymand and P. Linse, J. Chem. Phys. Vol. **112**, 14 (2000).

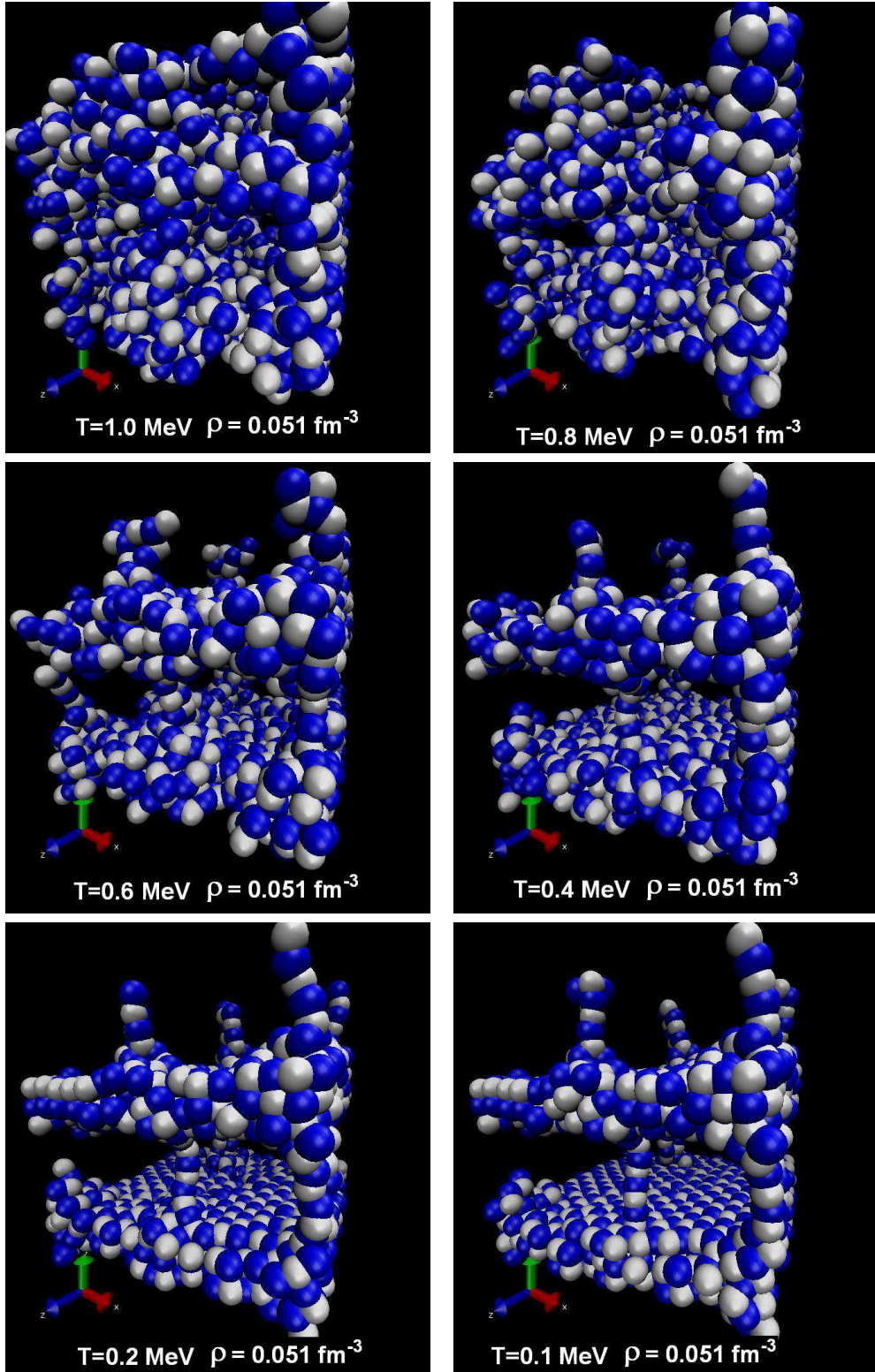


Figure 4. Configurations obtained with *CMD* with  $x = 0.5$  with the screened Coulomb potential for temperatures cooling from  $T = 1.0 \text{ MeV}$ , down to  $T = 0.1 \text{ MeV}$ .

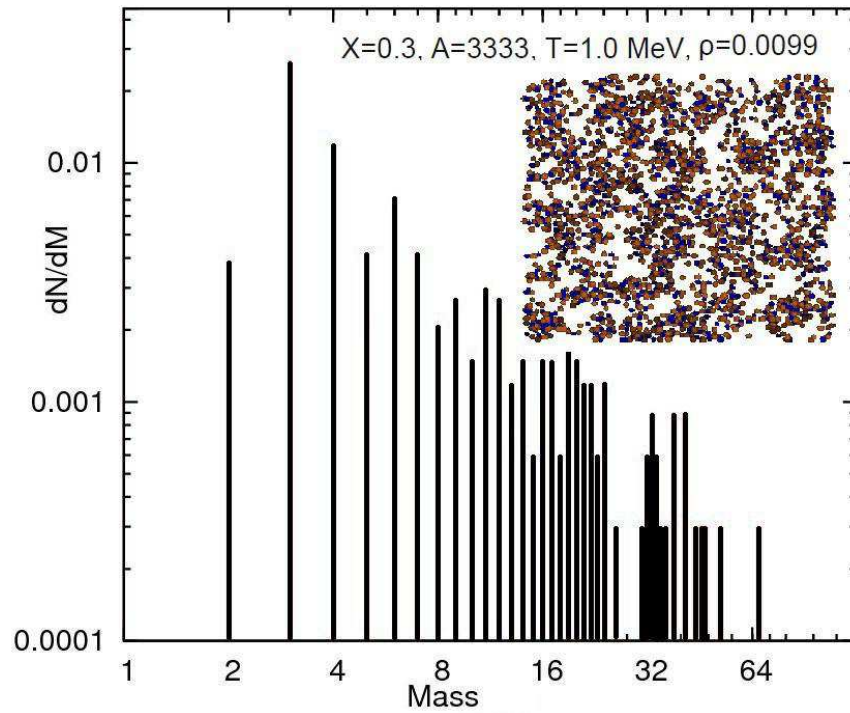


Figure 5. typical size distribution of clusters as obtained with *MST*. The inset shows a projection of the particle spatial distribution.

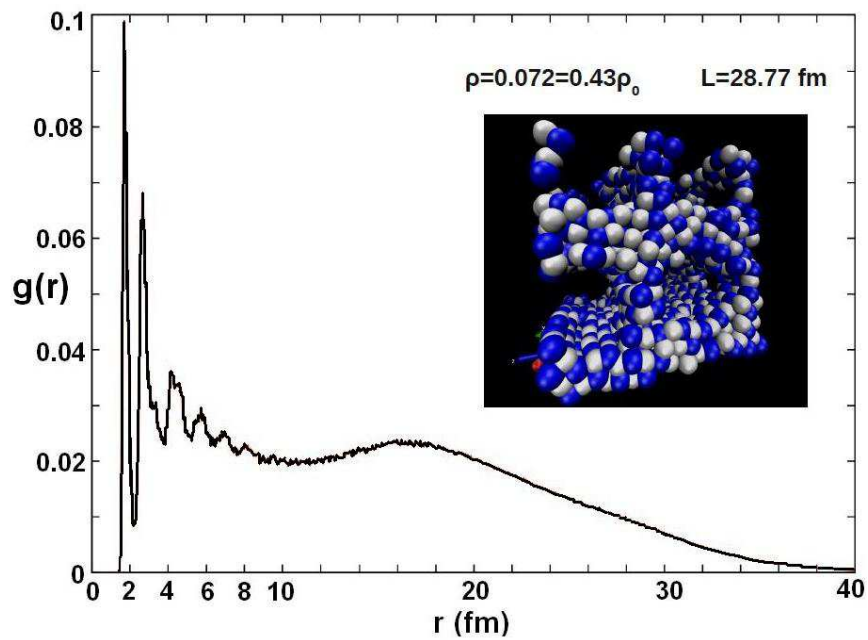


Figure 6. Typical radial distribution function. The inset shows the particle positions.

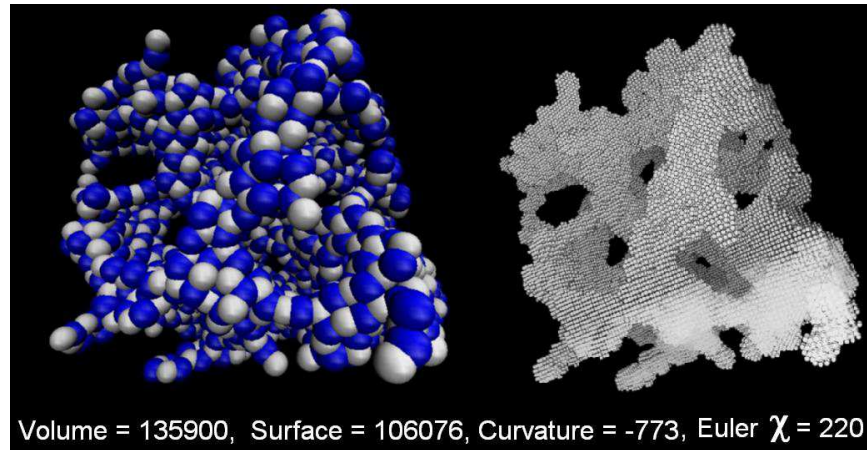


Figure 7. Typical nuclear structure and the grid used to calculate the Minkowski functionals. The structure corresponds to a case with  $x = 0.5$ ,  $\rho = 0.33 \text{ fm}^{-3}$  and  $T = 0.1 \text{ MeV}$ .

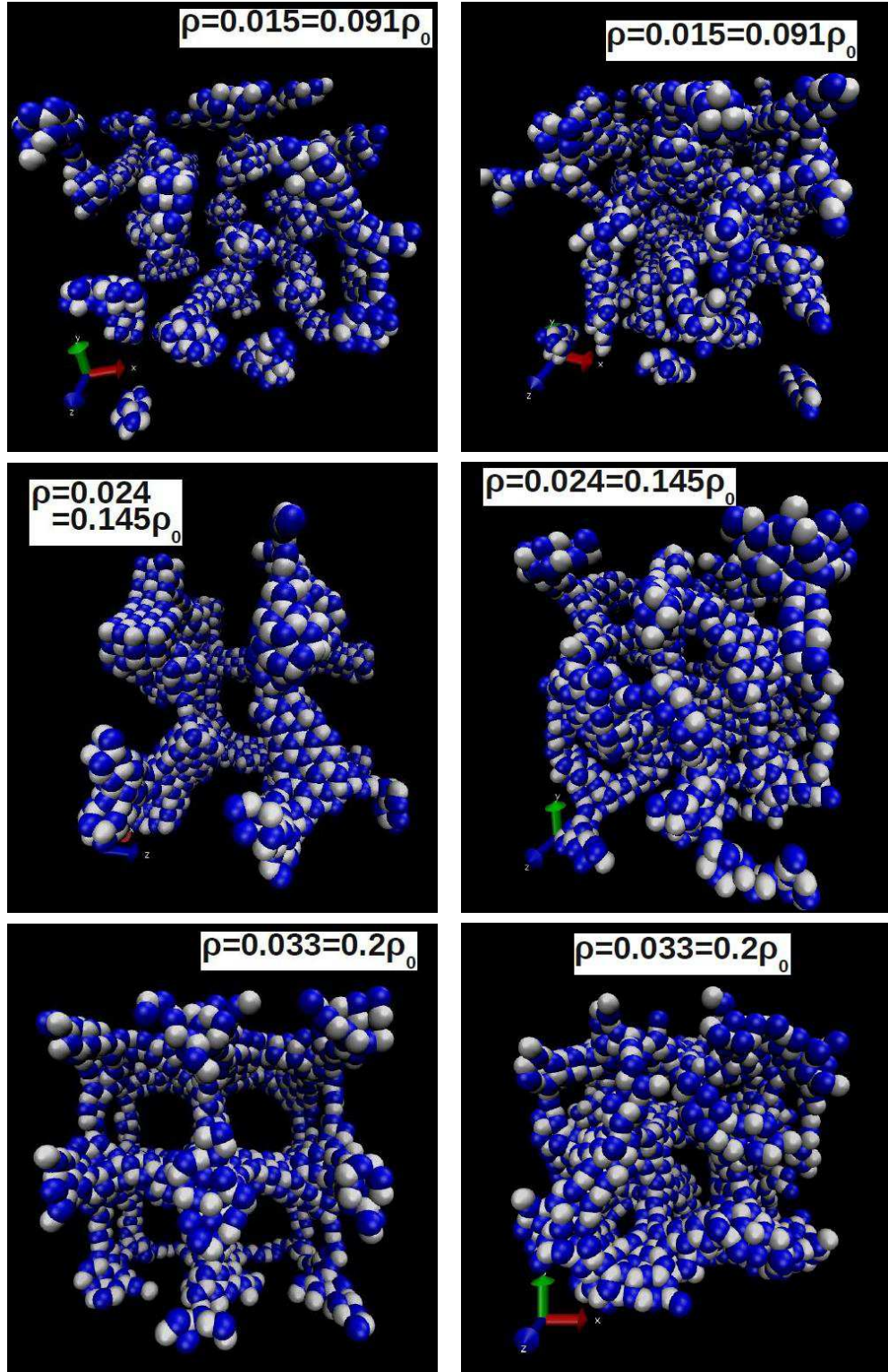


Figure 8. Configuration obtained with *CMD* with  $x = 0.5$ ,  $T = 0.1 \text{ MeV}$ , with the screened Coulomb potential (left figures), and with the Ewald summation (right figures).

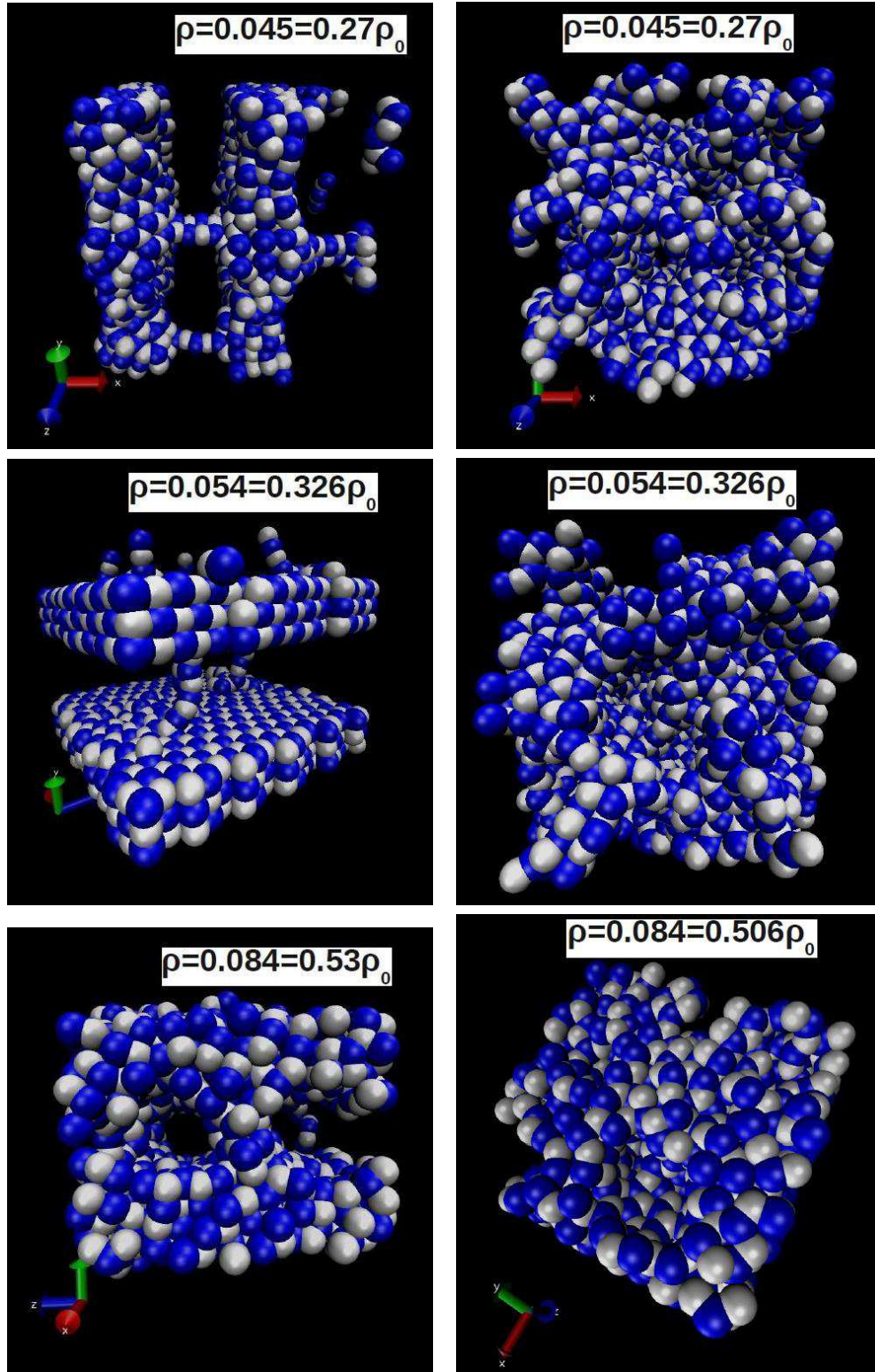


Figure 9. Configuration obtained with *CMD* with  $x = 0.5$ ,  $T = 0.1$  MeV, with the screened Coulomb potential (left figures), and with the Ewald summation (right figures).